The effects of short space and time scale current variability on the predictability of passive ichthyoplankton distributions: an analysis based on HF radar observations

J. A. HELBIG AND P. PEPIN*

Fisheries and Oceans, PO Box 5667, St John's, Newfoundland, Canada A1C 5X1

ABSTRACT

The importance of small scale variations in currents on the predictability of spatial distributions of fish eggs is investigated using dense observations of surface currents. The currents were measured with HF radar and used to drive an advection–diffusion model of ichthyoplankton concentration. We first demonstrate that the model produces acceptable agreement with observed egg fields. We then use the predicted egg fields as a basis for comparison with model runs made with currents subsampled in space and filtered in time. Significant error was found for spatial sampling intervals as small as 3 km, even though most of the variance in the currents occurred at much longer length scales. This was primarily due to the loss of the rich small scale variability in horizontal divergence. Nevertheless, most of the error is due to the misfit in the egg fields at larger length scales; that is, small scale forcing is necessary in this system for the larger scale features to be reproduced. This study thus suggests that considerable caution should be exercised before assuming that circulation models, even very sophisticated and detailed ones, capture enough of the variability of marine systems to make accurate forecasts of plankton distributions.

INTRODUCTION

The drift and retention of fish eggs and larvae within habitats critical to their survival are among the most poorly understood elements of the early life history of many fish (Sinclair, 1988). Failure to account for advective and dispersive exchange during ichthyoplankton surveys can lead to inaccurate population estimates as well as erroneous inferences about factors influencing mortality rates (Taggart and Frank, 1990; Pepin *et al.*, 1995; Helbig and Pepin, 1998a; Pepin *et al.*, 2002).

Numerical circulation models are often used in the planning, execution, and/or interpretation of these surveys, and these models span a great range of complexity and spatial resolution (e.g. compare McGillicuddy *et al.*, 1998; Proctor *et al.*, 1998). Moreover, these models are forced in a variety of ways (e.g. compare Davidson, 1999; Heath *et al.*, 1998) and are initialized with observed ichthyoplankton distributions of diverse quality (e.g. Bartsch, 1993; Pepin and Helbig, 1997). In order to establish how well surveys perform and to set appropriate confidence limits on survey results, it thus becomes necessary to understand how well models can predict the distribution of planktonic organisms.

Several questions are immediately evident: (1) At what spatial and temporal scales do currents need to be resolved in order to achieve an accurate forecast? (2) At what spatial resolution should the initial plankton distribution be observed, and how does the accuracy of this initial field affect the quality of the predictions? Finally, (3) what are appropriate measures of accuracy and predictability, and how do these relate to survey goals? Clearly, these questions are strongly linked, although the last is key in setting the other two.

For example, in population dynamics studies in which physical pathways are explored but absolute population estimates are not critical (e.g. Bartsch, 1993), it is only important that models reproduce the spatial distribution of plankton in an approximate or statistical sense. Thus, a drift model that resolved the most energetic spatial scales of motion, which was forced by seasonal mean currents, and that was initialized with an idealized plankton patch could be sufficient to estimate the fraction of eggs transported to a particular habitat (Bartsch, 1993; Hannah *et al.*, 2000). An appropriate measure of quality in this case could be the distance between the predicted centre of mass of the advected plankton field and the mean

**Correspondence*. e-mail: pepinp@dfo-mpo.gc.ca
Received 28 June 2000
Revised version accepted 8 November 2001

observed position. By contrast, in an egg survey designed for adult fish biomass estimation, one should have detailed knowledge of the spatial/temporal variability of the egg fields in order to interpret survey results (Helbig and Pepin, 1998a).

We report here on a study of the predicability of the spatial distribution of fish eggs in an embayment (Conception Bay, Newfoundland) using currents observed at high spatial-temporal density and egg concentrations observed at moderate spatial density. As the measure of quality, we chose the root mean square error between observed and predicted fields averaged over the bay. Surface currents were measured over a 15-day period with high frequency (HF) radar at hourly intervals and approximately 1 km resolution. Three plankton surveys were conducted at 6-day intervals, a temporal sampling rate biologically appropriate for organisms with short turnover times. The observed currents were used to force an advection–diffusion model in a series of simulations in which the spatial resolution and mean-to-variance ratio of the currents were manipulated in order to determine their influence on the accuracy of predicted changes in distribution.

The field study and model are described in the first two sections. A 'best-case' simulation is then presented to demonstrate that the model produces reasonable agreement with observed egg fields. As the number of plankton stations within the model domain was too small to resolve the small scale structure of the egg fields and to permit meaningful experimentation with sampling density, the best-case predicted plankton distribution was used as a basis for simulations in which the current field was subsampled in space and/or filtered in time. Although the effects of horizontal current divergence on plankton concentration are well known (Denman and Powell, 1984; Mackas and Denman, 1985), this study is distinguished from earlier ones by its detailed knowledge of the divergence field. Consequently, considerable emphasis is placed on understanding its role.

FIELD PROGRAM

Study site

Conception Bay (47.8°N, 52.8°W) is approximately 50 km in length and 25 km wide with a maximum depth exceeding 300 m and a total surface area of about 1000 km^2 (Fig. 1). A 150-m sill at the mouth separates the bay from the slightly shallower northern Grand Bank. Surface circulation is driven on short time scales (hours to days) by local winds and on longer time scales (weeks to months) by density driven exchanges with shelf waters and the inshore branch of the Labrador Current (deYoung *et al.*, 1993b; deYoung and Sanderson, 1995; Pepin *et al.*, 1995). In addition, storms are known to generate Kelvin waves trapped within about 5 km of either coast and whose associated currents have a jet-like character (deYoung *et al.*, 1993a, b; Davidson, 1999). Finally, it is likely that nonlinear effects generate much of the fine structure on the scale of the internal Rossby radius (~5–8 km) that is commonly seen in acoustic Doppler current profiler (ADCP) transects (J. Helbig, unpublished data; Davidson, 1999).

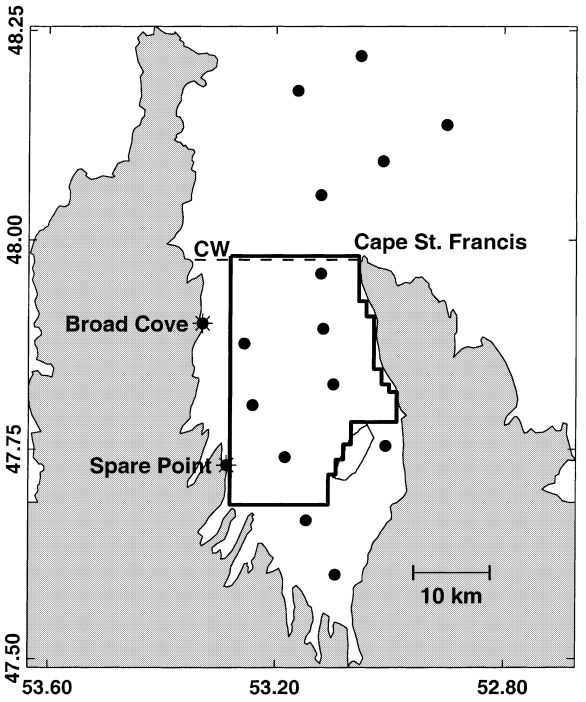

Figure 1. Plan view of Conception Bay showing plankton sampling sites (solid circles), HF radar stations (stars), and the model domain. The CW-line is coincident with the model's 'northern' boundary and extends westward to the coast.

Field survey

An experiment was conducted in the summer of 1991 over a 15-day period (July 3 to July 17: days 184–198) as indicated in Fig. 2. The survey was designed to (1) measure the distributions of ichthyoplankton (larvae and eggs of a number of species) and water properties (temperature, salinity, and fluorescence) within the bay at regular intervals, (2) simultaneously monitor currents throughout the bay, and (3) estimate the daily flux of water and ichthyoplankton across the open boundary

Figure 2. (a) Data return showing the number of radar vector current estimates per hour. The short horizontal lines demark the plankton survey times and the long line indicates the simulation period. (b) Winds observed at St John's airport.

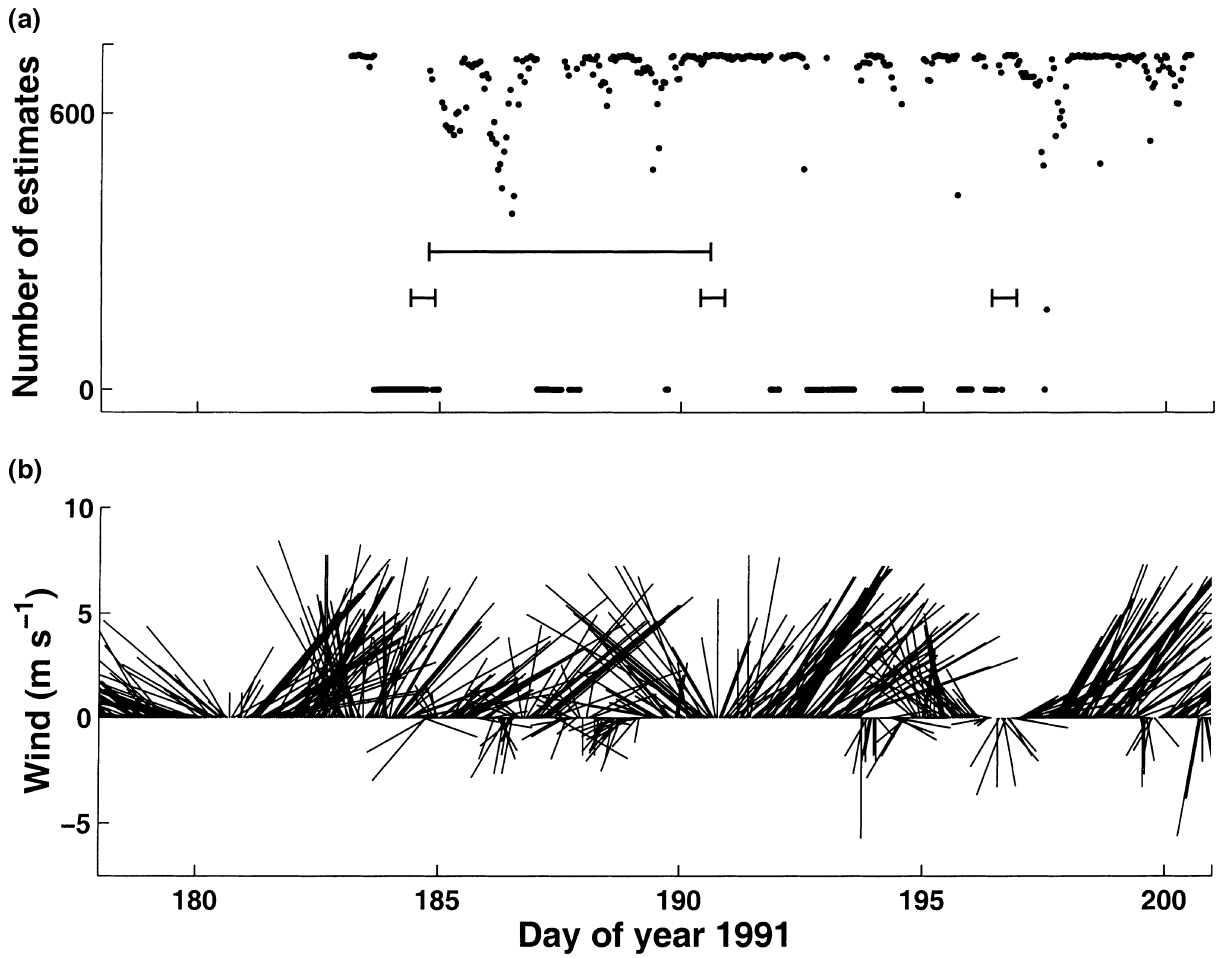

(Pepin *et al.*, 1995). Two vessels were used. CSS *Marinus* performed biological and water property measurements, whereas CSS *Shamook* undertook ADCP current measurements, occasional water property observations, and drogue tracking. Full-bay ichthyoplankton surveys were conducted every 6 days, whereas transects along the open boundary were carried out nearly simultaneously by both ships on an almost daily basis.

Both ships were available 12 h daily, and all biological sampling was conducted during daylight hours (07 : 00–19 : 00). Plankton samples were collected with a 4-m^2 Tucker trawl (see Pepin and Shears, 1997, for a discussion of capture efficiency). At each station, a single oblique tow of approximately 15 min was made at two knots (1 m s^{-1}). The tow depth of 40 m was chosen to sample the mixed layer (10–25 m) in which almost all the fish eggs and larvae reside (P. Pepin, unpublished data). Ichthyoplankton were sorted and identified to species or the lowest taxonomic level possible. Eggs were staged using the Markle and Frost (1985) scheme and development times were estimated from laboratory studies (P. Pepin, unpublished data). Abundance was calculated for each species, and abundance estimates were corrected for the number of eggs that could not be staged due to damage (< 5%).

In this study, we consider only fish egg distributions because eggs were the most buoyant plankton observed and the most abundant near the surface (P. Pepin, unpublished data) where the current observations are most meaningful. Moreover, their abundance can be measured with greater precision than other plankton (Pepin and Shears, 1997), their vertical distribution can be predicted from basic oceanographic data (Sundby, 1983), and they do not actively migrate vertically. Results are presented for American plaice (*Hippoglossoides platessoides*) because they were the most abundant species present.

Salinity and temperature profiles were made at each net station. Currents were measured with a 153-kHz RD Instruments acoustic Doppler current profiler (ADCP) as described in Colbourne *et al.* (1993) at depths exceeding 7 m. These currents provided comparative data for the radar (J.A. Helbig, unpublished data).

HF radar

Surface currents were monitored throughout the experiment by a pair of HF radars deployed and operated on the western side of Conception Bay (Fig. 1) by the Centre for Cold Ocean Research (C-CORE, Memorial University of Newfoundland). The principles of surface current detection using HF radar are well known (Crombie, 1955; Barrick *et al.*, 1977). Briefly, a series of omni-directional, ground-wave pulses are broadcast at each site over the water at near-zero incidence angle. These signals resonantly interact with surface gravity waves of wavelength half of that of the incident radar wave and are Doppler shifted from their transmit frequency by the component of the total surface current (wind wave phase velocity plus the ambient surface velocity) along the line of sight of the radar. Subtraction of the known shift due to wind waves gives an estimate of the radial surface current. Estimates from the two radars are then combined to form a vector current.

In our application, the two radars were detuned slightly from one another at a base frequency of 25.4 MHz to permit simultaneous operation, and they were run for 18-min periods on an hourly basis. The amplitude and phase of the backscattered signal was measured with a four-element, 1 m^2 receiver array located near each transmit antenna. This signal was time-gated to form a set of 40 18-min time series corresponding in range to a set of 1.2 km wide annuli centred on each radar site. Power spectra were computed for each time series, and each frequency estimate (near the main Bragg peaks) provided a single radial surface current estimate. The angular position within the appropriate annulus was estimated from the phase difference measured across the receive antenna using the Liese (1984) algorithm. This is the weakest part of the radar system. A least-squares algorithm robust to azimuthal errors was used to extract vector currents on a 1 by 1 km square grid from the combined radial speed estimates from each site. This procedure also provided estimates of divergence and vorticity. The 1 km resolution is somewhat smaller than the actual radar resolution of 1.2–2 km. The rms noise level in the currents was about 4 cm s^{-1} before filtering in time or space. Data return is indicated in Fig. 2.

Acoustic Doppler current profiler currents were measured daily along several transects across Conception Bay at depths extending from 7 m to the bottom. For most transects, there was good agreement with the radar-sensed currents. For others, the data clearly revealed large vertical shear in which the near surface current was dominated by the local wind.

MODEL

In three dimensions, the equation for the rate of change of plankton concentration $c(\mathbf{x}, t)$ is

$$\frac{\partial c}{\partial t} = -\mathbf{u}\cdot\nabla c - w\frac{\partial c}{\partial z} + K\left[\nabla^2 c + \frac{\partial^2 c}{\partial z^2}\right] + \nabla\cdot(K_H\nabla c) + \frac{\partial}{\partial z}\left(K_V\frac{\partial c}{\partial z}\right) - \frac{\partial w_c c}{\partial z} - \mathcal{Z}c + P \qquad (1)$$

and expresses the balance between advection, molecular and turbulent diffusion, buoyancy, mortality, and production. Here $\mathbf{x} = (x, y, z)$ with x pointing across the bay, y out of the bay, and z vertically upwards; $\mathbf{u} = (u, v, 0)$ is the horizontal component of the velocity; w is the vertical part; $\nabla = (\partial/\partial x, \partial/\partial y, 0)$ is the horizontal gradient operator; K is the 'molecular diffusivity' of the plankton and parameterizes the dispersion of plankton due to Brownian motion; K_H and K_V are the horizontal and vertical turbulent plankton diffusivities, which are generally several orders of magnitude larger than K and are generally space and time dependent; w_c is the buoyant ascent speed of plankton and can be specified in terms of organism shape and density and the ambient water density; $\mathcal{Z}$ is the biological mortality and can be space, time, and plankton density dependent; and P is a production term that allows for the generation of plankton or its passage from one stage to another. Ignoring molecular diffusivity and utilizing the incompressibility of the ocean ($\nabla\cdot\mathbf{u} + \partial w/\partial z = 0$), we can rewrite (1) in nondivergent form as:

$$\frac{\partial c}{\partial t} = -\nabla\cdot(\mathbf{u}c) - \frac{\partial}{\partial z}[(w + w_c)c] + \nabla\cdot(K_H\nabla c) + \frac{\partial}{\partial z}\left(K_V\frac{\partial}{\partial z}\right) - \mathcal{Z}c + P. \qquad (2)$$

Advection now appears as part of the divergence of the plankton flux.

We consider the typical field situation in which tows of a fixed depth h_t are made, for which h_t exceeds the maximal depth at which plankton are found. Vertically integrating (2) over h_t and applying the

boundary conditions that (1) the buoyant and turbulent fluxes of plankton across the sea surface interface vanish, and (2) that the plankton concentration is zero at $z = -h_t$, we obtain an equation for the vertically averaged plankton concentration $\bar{c}(x, y, t)$,

$$\frac{\partial \bar{c}}{\partial t} = -\nabla \cdot (\overline{\mathbf{u}c}) - K_H \nabla^2 c - Z\bar{c} + \bar{P}. \qquad (3)$$

In doing so, we have assumed that the turbulent diffusivity K_H is constant and have avoided any issues of differential mortality by fixing Z as constant in space and time. These commonly made assumptions are not necessarily good, but we do not have data to support better ones. Finally, we focus on a single stage of plankton by setting $P = 0$.

The vertical average of the horizontal plankton flux, $\overline{\mathbf{u}c}$, cannot be computed from the field data. Rather, we parameterized it in terms of the variables we did measure as

$$\overline{\mathbf{u}c} = r\mathbf{u}_r\bar{c} \qquad (4)$$

where $\mathbf{u}_r$ is the radar sensed velocity and $r = 0.4$. The validity of this parameterization is discussed later. Thus we can finally write an equation for the mortality-corrected, vertically averaged plankton concentration, $C(x, y, t) = e^{Zt}\,\bar{c}(x, y, t)$, that can be applied to our field data:

$$\frac{\partial C}{\partial t} = -r\nabla \cdot (\mathbf{u}_r C) + K_H \nabla^2 C. \qquad (5)$$

Equation 5 was solved on an Arakawa C-grid (Arakawa, 1966) using standard second-order, centred in space, centred in time, finite differences (Roache, 1985), with the radar grid points defining the mesh corners. A timestep of 5 min was used. Although their number was very small, missing radar currents were interpolated or extrapolated as necessary using a circularly symmetric, spatial filter with a 5 grid radius. As described later, the model was initialized with a plankton field optimally interpolated onto the model grid. K_H was fixed at 35 $m^2\ s^{-1}$, below the range of 70–100 $m^2\ s^{-1}$ estimated for Conception Bay from drifting buoy data by deYoung and Sanderson (1995). This smaller value is consistent with the model grid scale and is as small as model stability permitted.

Consider now the parameterization (4). The current measured by the radar is a weighted average over a depth scale defined by the wind wave wavelength $\lambda = 5.9$ m (Stewart and Joy, 1974; Ha, 1979),

$$u_r = (\pi/\lambda)\int_{-\infty}^{0} e^{(\pi z/\lambda)} u(x, y, z, t)dz \qquad (6)$$

The vertical distribution of fish eggs in Conception Bay can be reasonably described as exponential, $c(x, y, z, t) = c_o(x, y, t)e^{z/h_p}$, with an e-folding depth of $h_p \approx 25$ m (P. Pepin, unpublished data). Consistent with the ADCP measured velocity, we assume the upper layer current can be similarly represented with an e-folding scale h_u of about 30 m. From (4), we find that for $h_p = 25$ m and h_u in the range of 10–50 m, r varies between 0.37 and 0.77. The value $r = 0.4$ is thus at the low end of the scale, but is reasonable. As described in the next section, it was chosen because it gave the best, albeit partially subjective, agreement between predicted and observed egg fields. From an alternate viewpoint, $\overline{\mathbf{u}c}/\bar{c}$ is the mean velocity experienced by an average fish egg and is a fraction r of the near-surface, radar-sensed current. The parameterization specifies that this mean current has the same direction as that measured by the radar. This assumption is consistent with the ADCP data which show little directional shear in the upper layer below 7 m (the uppermost bin). A least-squares fit of the ADCP current at 7 m to the radar current, $\mathbf{u}_{adcp} = \mathbf{u}_o + \alpha\mathbf{u}_r$, explained 55% of the observed variance in $\mathbf{u}_{adcp}$ and gave $|\alpha| = 0.48$, an anticlockwise turning angle of 18°, and $\mathbf{u}_o \approx 0$.

At closed boundaries, the model permits no advective or diffusive flux into or out of the model. At open boundaries, the normal gradient of egg concentration is set to 0 at the boundary. That is, the value of c just outside the boundary is set equal to that just inside the boundary. Thus an outflowing current expels matter at the modelled concentration, whereas an inflowing current injects material into the model, but at the same concentration as already exists in the boundary cell. Mass is not conserved. However, no matter can diffuse across an open boundary.

Although daily egg surveys were made across several transect lines including the opening to the bay (line CW; Pepin *et al.*, 1995), the data were not sufficient to specify egg concentrations on all the open boundaries. Some testing was carried out specifying the concentration on the seaward boundary, but the results obtained were not significantly different from those reported here.

No open boundary conditions were imposed on the currents as the domain of valid radar-derived currents is slightly larger than the model.

RESULTS

Observations

To prepare to describe the simulations, we first describe the observed plankton fields and the spatial and temporal structure of the current and divergence fields.

Mean currents over the simulation period were generally weak (< 5 cm s^{-1}) and described a broad anticlockwise gyre with an intensified outflow (10–25 cm s^{-1}) along the north-eastern coast (Fig. 3b). As noted by deYoung and Sanderson (1995), mean currents in Conception Bay are generally small compared with fluctuations even though the tidal contribution is minimal (~3 cm s^{-1}), and Fig. 3a shows this was the case except in the coastal jet. There was a distinct spatial pattern in the mean

Figure 3. (a) Current variance for the simulation period of 5–9 July. Each cross is aligned with the principal axes of variation and each arm has a length equal to the standard deviation. (b) Mean velocity field for the simulation period. (c) Standard deviation of the horizontal divergence for the simulation period in units of 10^{-5} s^{-1}. (d) Mean divergence for the simulation period; dark and light shades indicate convergence and divergence, respectively.

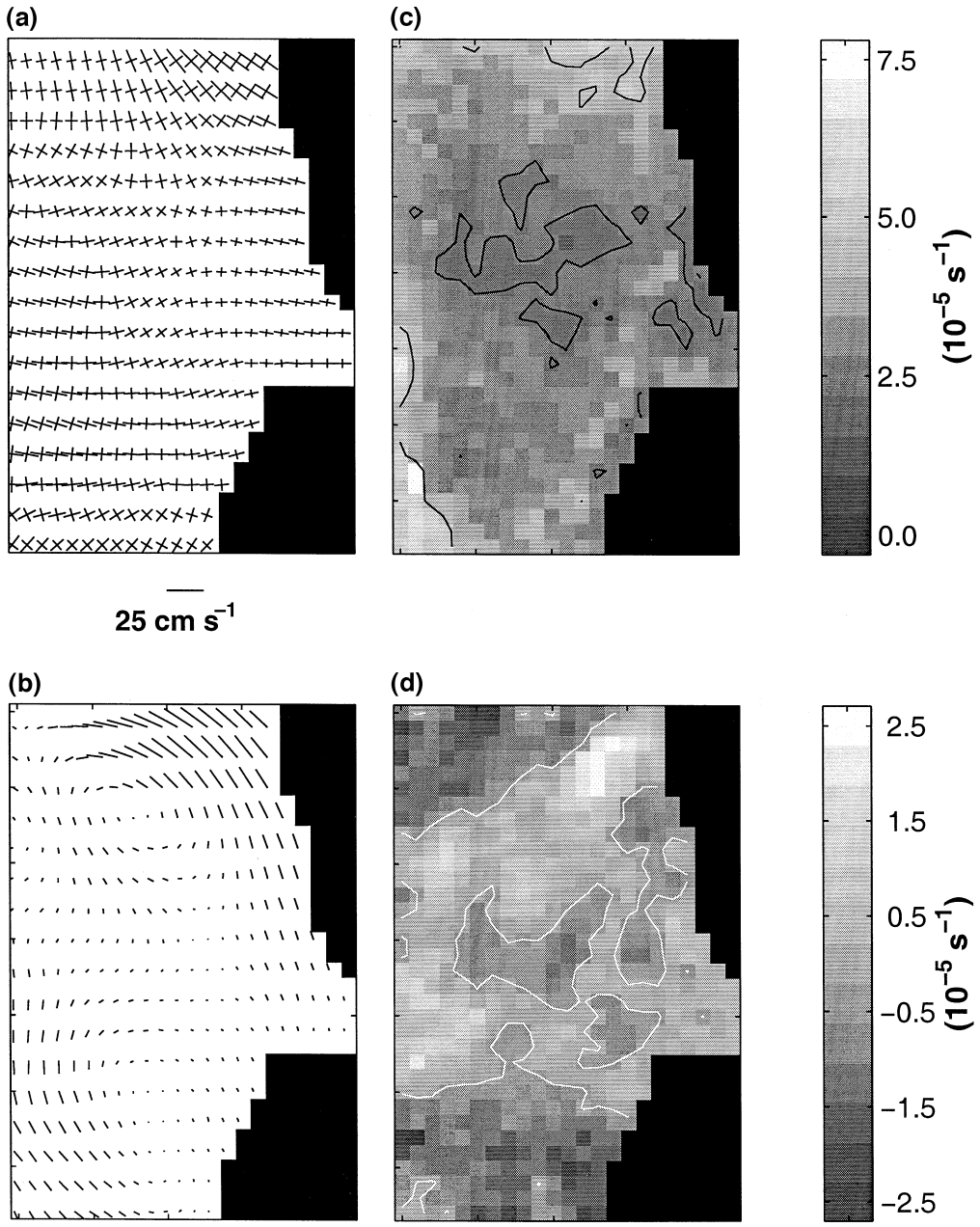

divergence field (Fig. 3d); regions of significant convergence ($D < -1.5 \times 10^{-5}$ s^{-1}) in the north and south were separated by a broad zone of net divergence. A strong divergence cell ($D > 1.5 \times 10^{-5}$ s^{-1}) occurred in the north-east corner where the jet separated from the coast (Cape St Francis). Regions of peak divergence/convergence were closely associated with regions of high variability in the current velocity (Fig. 3a,c).

Divergence will prove to play an important role in the modelling of egg distributions, so it is useful to understand some of its dynamics. In Conception Bay, divergence is largely a coastal phenomenon attributable to upwelling (Davidson, 1999) and to spatial inhomogeneities in the wind. The traditional ecological knowledge of the local fishing community tells us, for example, that winds are enhanced near Cape St Francis by the roughly 50 m high cliffs there.

The along- and cross-bay velocity wavenumber spectra are all red (Fig. 4a), and are well fit over the length range of 4–18 km by a k^{-2} relationship, where k is the along-bay or cross-bay wavenumber (2π/length scale). The spectra are not isotropic especially at longer length scales (as is also evident from Fig. 3). By contrast, the divergence spectra are not red as they decrease toward smaller wavenumbers after peaking at a wavelength of about 8 km, roughly the upper estimate of the internal Rossby radius. Relative to the current spectra, the divergence spectra are rich at small wavelengths $S_D \sim k^2 S_{u,v}$.

The u and v frequency spectra are broadly peaked about a period of 20 h encompassing a diurnal

Figure 4. Current and horizontal divergence spectra. (a) Log–log nonvariance preserving plot of along- and cross-bay wavenumber spectra. The first inset shows slopes for spectra proportional to k^{-1} and k^{-2}. A second inset illustrates the 95% confidence intervals for the spectrum estimates. (b) Semi-log variance preserving plot of the frequency spectra. $S_{uv}(k_x)$ and $S_{uv}(k_y)$ have units of m^3 s^{-2}, $S_D(k_x)$ and $S_D(k_y)$ have units of m s^{-2}, $S_{uv}(f)$ have units of m^2 s, and $S_D(f)$ has units of s^{-1}.

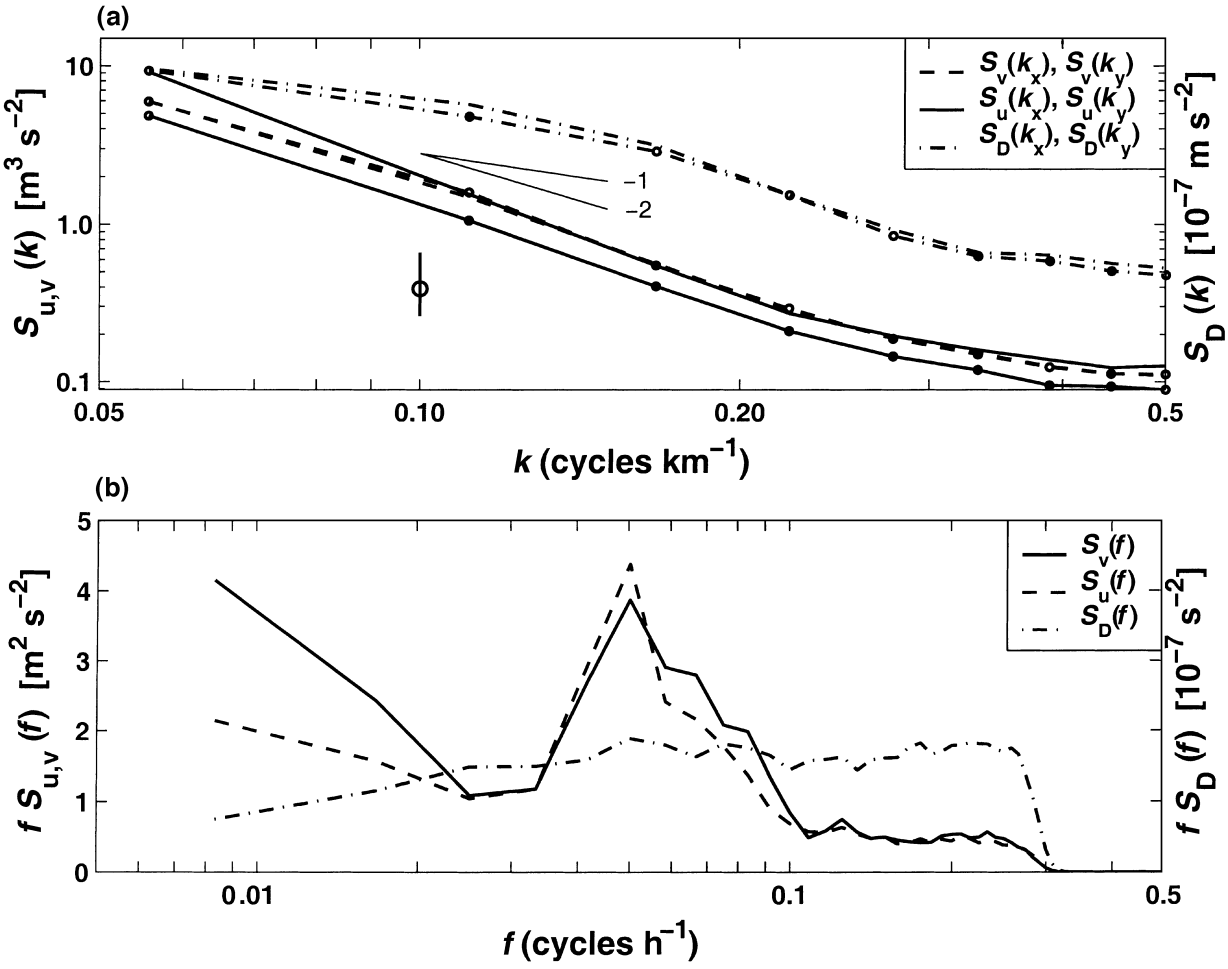

circulation forced by land–sea breezes, inertial oscillations, and the tides (Fig. 4b). A broad, low-frequency peak due to wind forcing is also evident, although winds during the study were relatively weak (Fig. 2). Again by contrast, the divergence frequency spectrum is relatively white and does not exhibit either of the peaks in the current spectra.

Egg concentrations were optimally interpolated onto the model grid (Bretherton *et al.*, 1975) using observations from all 14 stations. An isotropic exponential autocorrelation function with an *e*-folding length of 7.5 km was used in accord with that computed by Helbig and Pepin (1998b). The interpolated Stage I plaice egg field was broadly distributed at the start of the study period with the highest concentrations at the head of the bay along Bell Island (Fig. 5a). The predicted mean square error in this estimate displays a 'bull's eye' pattern characteristic of fields observed at a scale greater than their correlation length (Fig. 5b). That is, the survey was not dense enough to resolve fine scale structure in the egg field, and the resultant initial field is overly smooth. We address the significance of this for the simulations later.

At the observed temperatures, Stage I eggs found at the start of the study would have reached the third stage of development after 6 days (P. Pepin, unpublished data) and appear to have been more patchily distributed (Fig. 5c). Peaks in abundance of Stage III eggs occurred at the south-eastern and north-western extremities of the bay, and the overall abundance decreased by ~65% (similar to other estimates of natural mortality of about 0.15 day^{-1}). A region of

Figure 5. (a) Optimally interpolated initial (5 July) egg distribution; (b) estimated error; (c) optimally interpolated final (9 July) egg distribution; and (d) 'best' simulated final egg distribution scaled for mortality.

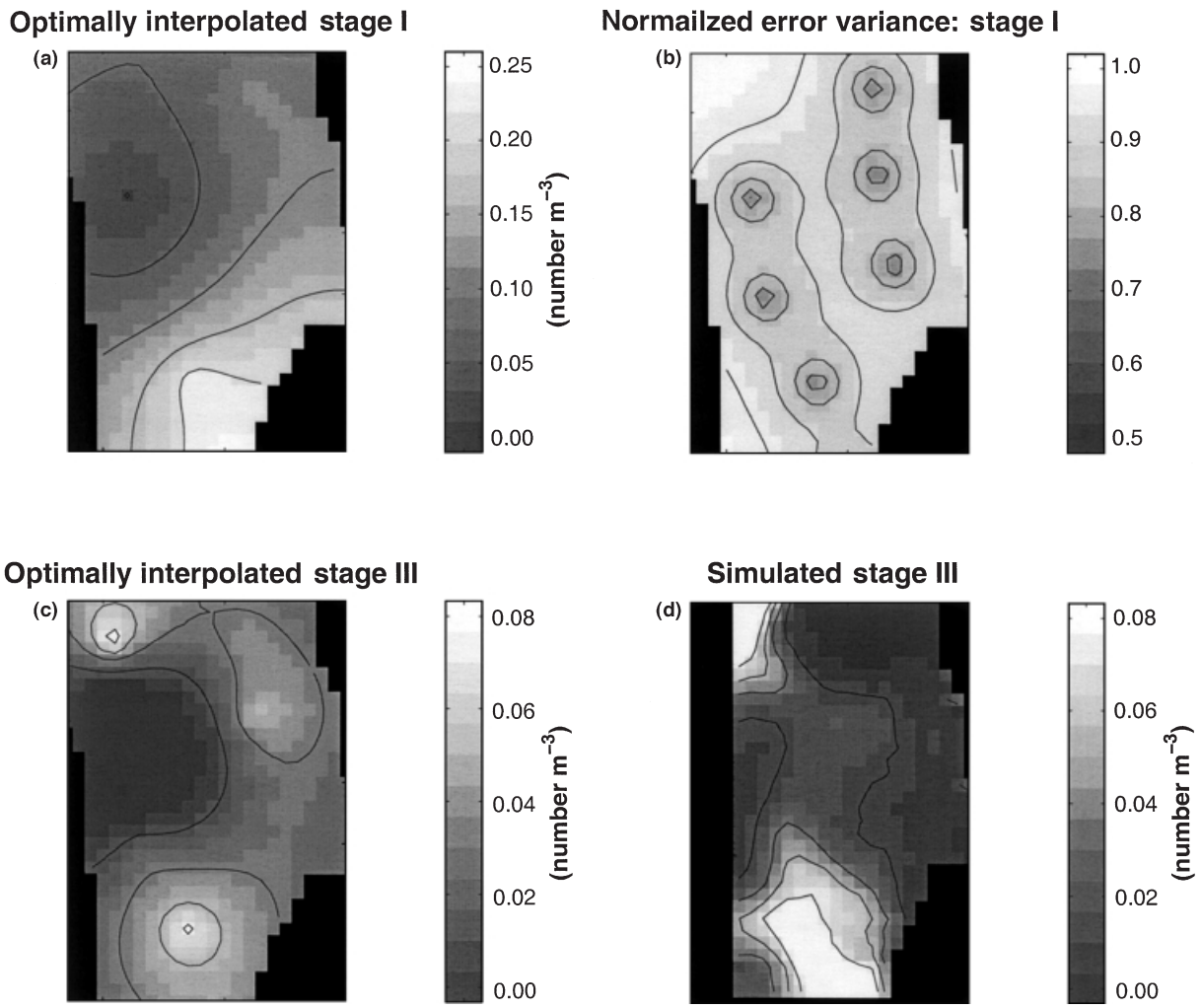

very low abundance of Stage III eggs in the central western bay coincided with that observed for Stage I eggs during the first survey.

Best-case simulation

A series of runs with $0 \leq r \leq 1$ was made, and the fit between predicted and observed plaice egg distributions was judged objectively by the correlation between the observed and predicted values at the six stations within the model domain. The best fit was obtained for $r = 0.4$ ($R^2 = 0.53$) and represented a broad maximum in R^2 extending from about $r = 0.25$ to $r = 0.5$. The predicted final field (Fig. 5d) bears a strong resemblance to the optimally interpolated final field. In particular, the model reproduces the peak in the north-west corner, a peak at the head of the bay, and a zone of low concentration in between, although it also predicts a zone of very low concentration in the north-east that is not observed. In addition, once the model field is adjusted for mortality, the predicted magnitudes are similar to those observed. We conclude that the model produces a plausible result. Given the plankton sampling density, however, we emphasize that this is a partially objective conclusion and stress only that the results are plausible.

The predicted final field also bears a marked resemblance to the mean divergence (Fig. 3d): both abundance peaks lie in mean convergence zones, and the relatively sparse area separating them coincides with the large region of mean divergence. Examination of Fig. 6, which shows a progression of egg field snapshots, reveals a number of features that are clearly attributable to divergence. For example, the concentration increase in the south-west corner at hour 120 is obviously associated with a strong convergence cell. On the other hand, there also exist features that are just as clearly advective, like the northward drift of eggs near the model centre at hour 72 or the flow of low concentration water in the north-east at hour 120. These features are even more evident in Fig. 7 which shows individual forward and backward particle paths overlaid on the initial and final egg fields. Examination of this figure convincingly demonstrates that the dominant features in the predicted final field are not associated with the open boundary.

The right hand side of eqn 5 can be rewritten as $-r\mathbf{u} \cdot \nabla c - rc\nabla \cdot \mathbf{u} + K_H \nabla^2 c$ to explicitly separate advective and divergent effects. Each of these three terms was evaluated at a number of grid points, and all play important roles that vary with time and with location. Consider, for example, the north-west corner. Convergence establishes a small abundance peak very early (24 h) and then acts for most of the remainder of the simulation to concentrate the eggs. Advection transports particles out of this region almost continuously. The open boundary plays no significant role as is clear from Fig. 7c. Similarly, the area of the north-east corner is one of almost continuous advective loss that dominates a relatively weaker and oscillatory convergence. When convergence becomes strong late in the simulation, the egg field is so dilute that it remains so. Consider finally, the area of high concentration at the head of the bay. For the first 96 h, it is an advective source, but this advection is partially counterbalanced by convergence. During the final 48 h advection and convergence both act to increase concentration.

In general, but not always, divergence and advection play opposing roles. However, the important point is that divergence is important for this system and should not be ignored. In areas of large horizontal shear, diffusion partially compensates for advection, as the currents stir plankton patches thus sharpening concentration gradients and increasing the diffusive flux. Otherwise, diffusion generally plays a minor role.

Simulations using degraded forcing

In order to explore the questions posed in the introduction, we executed a set of simulations in which the forcing currents were degraded in time or space. However, the number of stations within the model domain was too small to allow us to evaluate these experiments using the observed plankton fields; both the optimally interpolated initial and final fields lack the small scale structure of the true fields. Consequently, we adopted the best-case final predicted field as our basis for comparison. This field is plausible and we assume that it is realistic, i.e. that it could exist in nature. Of course, it too lacks the very small scale structure found on subgrid scales (< 1 km), and our conclusions will be therefore somewhat conservative. We retained the optimally interpolated Stage I field as our initial field. We chose our measure of model accuracy, denoted here as ϵ, to be the root mean square error between the predicted and base fields averaged over the full model grid and normalized by the standard deviation of the base field.

Temporal degradation was achieved by passing the currents through a set of low-pass filters (Fig. 8). Spatial degradation was achieved by subsampling the observed fields at a set of stations uniformly distributed over the model grid but with spacings that were a multiple of 1 km. The subsampled currents were then bilinearly interpolated back onto the full 1 km grid.

In addition, the effects of degrading the current field obviously depend strongly on the relative

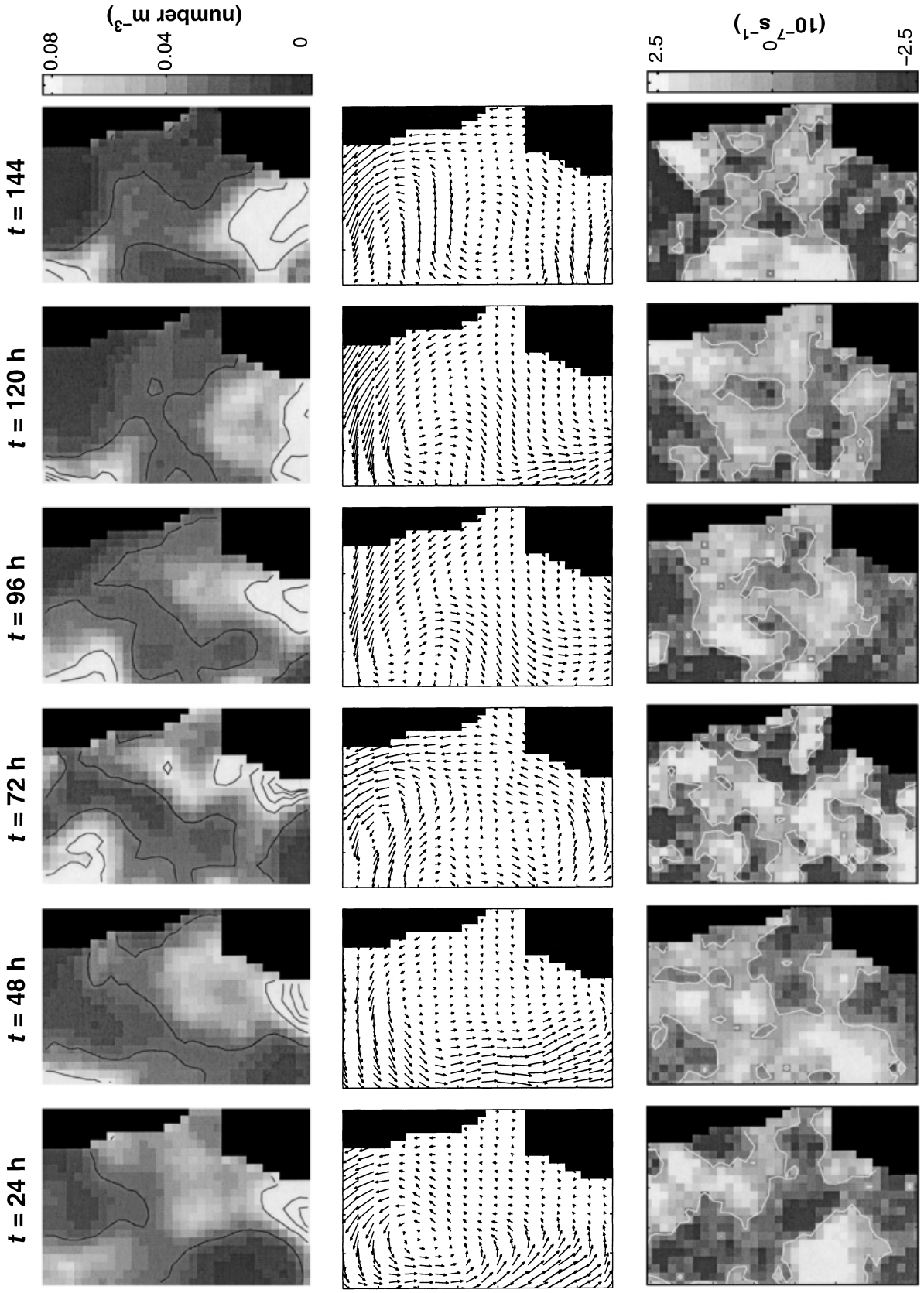
(number m⁻³)
0.08
0.04
0
(10⁻⁷ s⁻¹)
2.5
0
−2.5
t = 144
t = 120 h
t = 96 h
t = 72 h
t = 48 h
t = 24 h

Figure 6. (a) Daily snapshots of spatial egg distributions for the best case simulation. (b) Mean velocity fields averaged over the 24 h preceding the snapshot. (c) Mean horizontal divergence fields (in units of 10^{-5} s^{-1}) averaged over the preceding 24 h; dark and light shades indicate convergence and divergence, respectively.

strengths of its mean and fluctuating components, as their spectral characters differ. Indeed this is tautological for temporal filtering in which the mean is defined as a time average. We consider three cases: the observed currents (case 1M), the currents minus their temporal mean (case 0M), and the currents with their mean enhanced by a factor of three (case 3M).

To establish a level of significance for ϵ and to try to address the importance of the accuracy of the initial plankton field, we ran a set of 100 simulations in which the initial plankton field contained realistic levels of sampling error. Specifically, for each simulation, the 14 observed values were contaminated with zero-mean Gaussian noise having a variance in accord with the observations (Pepin and Shears, 1997) to give a new set of 'observations' just as likely as the set actually observed. These sets were then optimally interpolated to create 100 fields that were used to initialize the model runs. The resultant ϵ averaged over the 100 simulations was about 0.10 (Fig. 9). The

Figure 8. Frequency spectra, $S_v(f)$ of the temporally filtered along-bay current. Labels serve as references for filters referenced in Fig. 10.

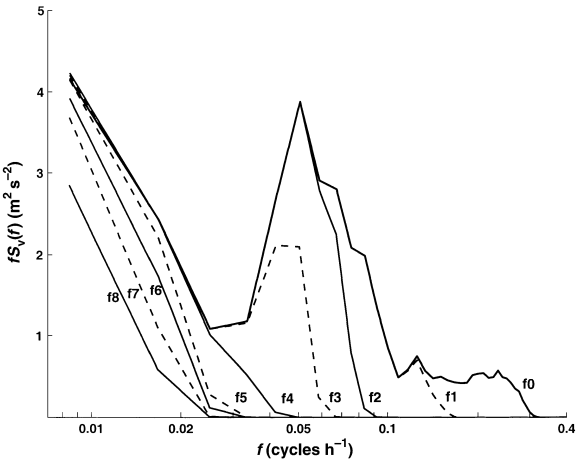

distribution of ϵ was positively skewed, with the upper 95th percentile at approximately twice the mean, consistent with expectations for patchily distributed organisms. Consequently, in the interpretation of the simulations made with degraded currents, ϵ was considered significant if it exceeded 0.1.

As expected, predictive quality decreases steadily as the degree of temporal damping increases (Fig. 10a). For cases 0M and 1M, ϵ exceeds the 0.1 threshold if

Figure 7. (a and b) Particle forward drift tracks superimposed on the final simulated field. (c) Particle backward drift tracks superimposed on the initial field. Grey scales are as in Fig. 5.

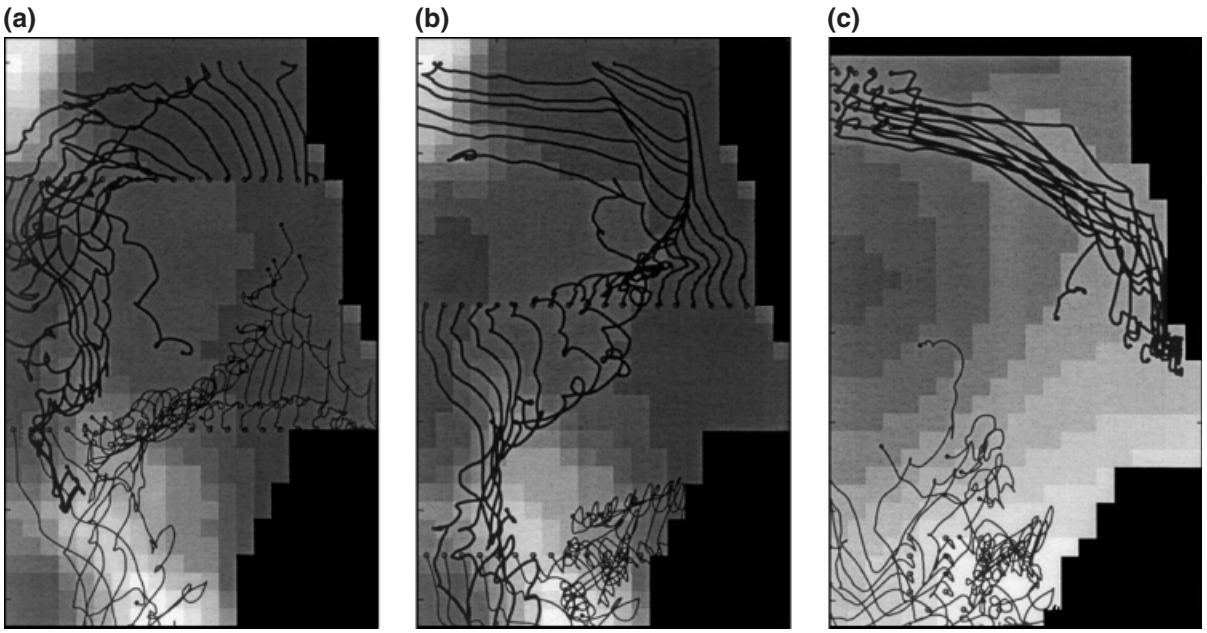

Figure 9. Histogram of the relative root mean square error ϵ found when the initial plankton field was contaminated with noise in 100 simulations.

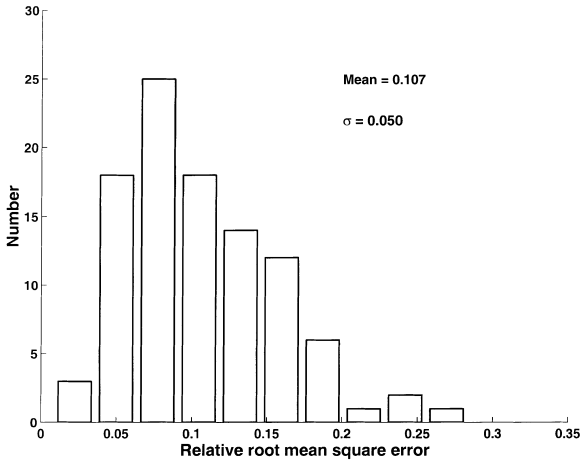

variability with periods greater than about 7 and 14 h, respectively, is suppressed (cf. Fig. 8). For case 3M, temporal filtering has little effect until periods of approximately 50 h are suppressed. The stronger the mean, of course, the better the prediction. The effects of spatial subsampling are more dramatic and are not as dependent on the relative strength of the mean (Fig. 10b). In fact, when the sampling interval is doubled to 2 km, ϵ exceeds the 0.1 mark in all three cases. Thereafter, the error increases steadily. The reason for the rapid decrease in quality is largely due to the high wavenumber content of the divergence (Fig. 4). As the sampling interval increases, the relative strength of the divergence field decreases more quickly than that of the current field, and the features in the base final fields that depend on divergence, like the north-west corner patch, do not appear.

DISCUSSION

Although our knowledge of both currents and plankton distributions is imperfect, recent developments in fisheries oceanography (e.g. Werner *et al.*, 1996; Heath and Gallego, 1998) may tempt us to believe that our understanding of the physical environment is adequate to permit accurate predictions of the spatial distribution of plankton. The results of this study suggest that considerable caution should be exercised before assuming that circulation models, even very sophisticated and detailed ones, capture enough of the variability of marine systems to make accurate forecasts of plankton evolution.

In the Introduction, we posed three basic questions that addressed spatial and temporal resolution, the accuracy of initial fields, and the choice of a measure of quality. We indicated that the answers were dependent on the system of interest as well as on logistical constraints. As the present study is most relevant to the design of egg surveys used to estimate adult fish biomass, we restrict our discussion accordingly. We also note that, although ϵ was a natural choice for this study that allowed us to quantify our conclusions (some of which might seem rather obvious otherwise), other choices might be more meaningful in other situations.

Our results indicate that ϵ depends more strongly on the spatial sampling rate than it does on the temporal one (Fig. 10). We found appreciable error in all three cases (0M, 1M, 3M) for sampling intervals as small as a few kilometres; ϵ thereafter increased almost linearly, even though the most of the variance in the currents occurred at longer length scales (Fig. 4). This is primarily due to the loss of small scale variability in horizontal divergence which compresses plankton patches. Notwithstanding this, most of the error is due to misfit at larger length scales. (The final plankton fields display a k^{-2} – like spectrum in concert with their step-like character.) That is, small scale forcing is necessary in this system in order for the larger scale features to be reproduced. Relatively little difference was found between the three cases studied.

The effects of temporal degradation were less dramatic and it was not until filtering depleted the spectral peak centred on 20 h that the predictions appreciably deteriorated. Of course, not all systems will be more sensitive to spatial than to temporal resolution. For a counterexample, one need only consider a tidally driven fjordic estuary in which both cross- and along-fjord fluctuations are small compared with temporal ones. Moreover, achieving high temporal resolution in the field is not an issue, unless one relies on shipboard ADCPs. But spatial resolution is. Thus the simulations using spatially degraded currents are of far greater practical interest. Consequently, we conclude that if either the sampling strategy for an egg survey or its subsequent interpretation are dependent on a prediction of egg distribution, then the fine scale features of the circulation must be resolved – at least for systems in which horizontal divergence is likely to be appreciable. The only realistic way to achieve this resolution is either with high-density radar based measurements (for highly buoyant species) or with a fine meshed numerical model that assimilates appropriate observations (perhaps including radar) (e.g. Bowen *et al.*, 1995; Taggart *et al.*, 1996; Lynch *et al.*, 1998).

By contrast, we found relatively little impact on predictive skill due to perturbations of the initial

Figure 10. Relative root mean square error ϵ as a function of (a) temporal filter and (b) spatial sampling interval for observed currents (case 1M, solid lines), demeaned currents (case 0M, dashed lines), and currents with an enhanced mean (case 3M, dash-dotted lines). Temporal filter labels are identified in Fig. 8. The mean rms error associated with uncertainty in the initial plankton field is 0.1.

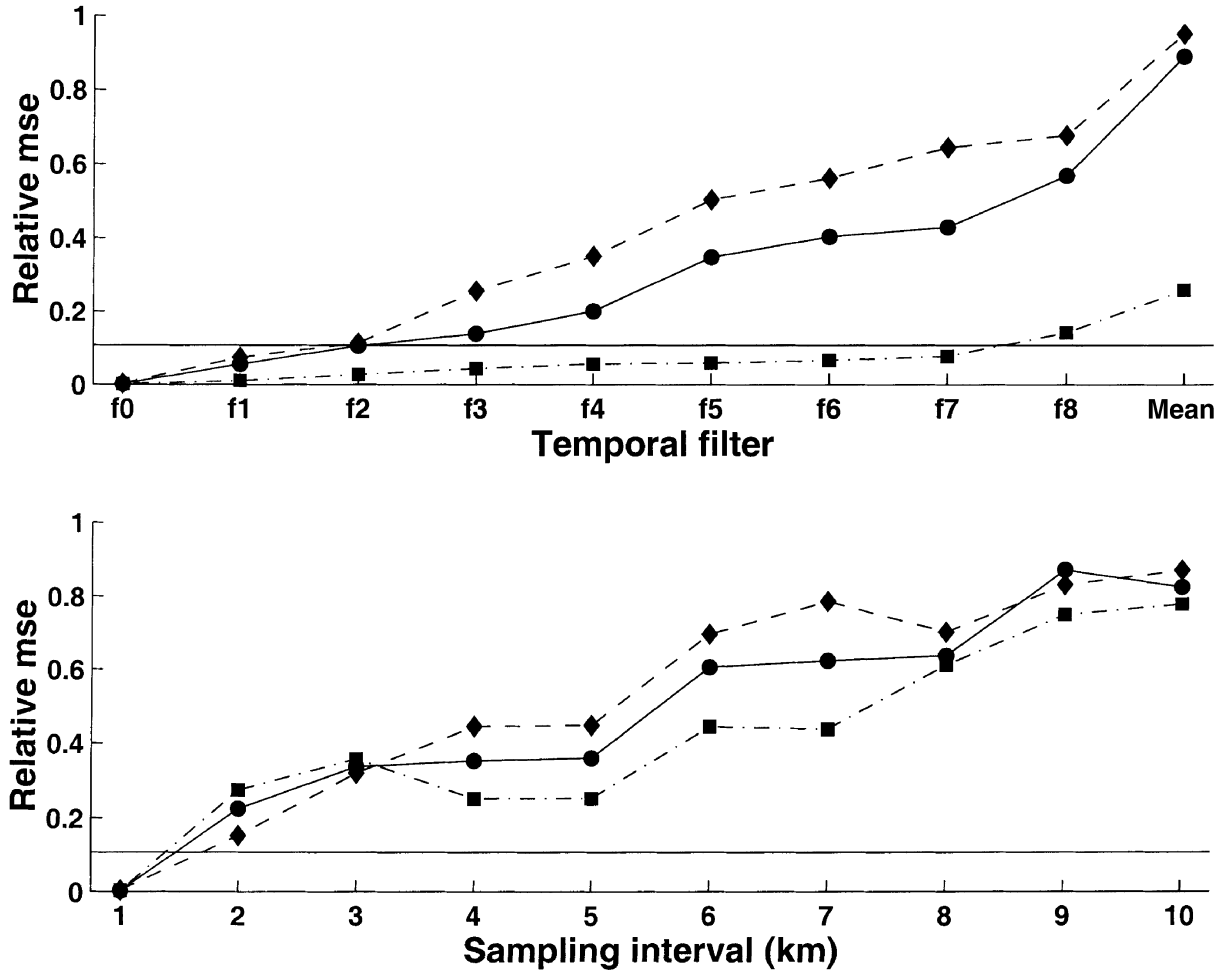

plankton field. This is largely due to the importance of the divergence field in establishing the high concentration zone in the north-west corner fairly early in the simulation (Fig. 6). All that was really required was a seed population in the area.

This study represents an extreme case in which a weak mean current field is dominated by fluctuations. In systems with strong mean circulation patterns or in which the variability is largely deterministic (i.e. tidal), predictions of transport and dispersion would have greater certainty. However, our results highlight the importance of knowing the small scale horizontal divergence.

From a broader perspective, our results are relevant to the modelling of the early life history of fish. Biophysical models that include drift, growth and differential mortality in addition to transport and dispersion are limited by uncertainty in currents as well as to incomplete knowledge of biological dynamics of the plankton (e.g. spatial patterns in mortality). Progress in understanding the impact of transport on the early life history dynamics of fish will require that the stochastic elements in each of these be considered.

ACKNOWLEDGEMENTS

We wish to thank E. Colbourne, R. Laprise and T. Shears for their assistance in the field. We also thank Dr J. Largier for his very constructive comments as a referee. This project was partially funded by the Northern Cod Science Program of the Department of Fisheries and Oceans.

REFERENCES

Arakawa, A. (1966) Computational design for long-term numerical integration of the equations of fluid motion: two-dimensional incompressible flow. Part I. *J. Comput. Phy.* **12**:12–35.

Barrick, D.E., Evans, M.W. and Weber, B.L. (1977) Ocean surface currents mapped by radar. *Science* **198**:138–144.

Bartsch, J. (1993) Application of a circulation and transport model to the dispersion of herring larvae in the North Sea. *Cont. Shelf Res.* **13**:1335–1361.

Bowen, A.J., Griffin, D.A., Hazen, D.G., Matheson, S.A. and Thompson, K.R. (1995) Shipboard nowcasting of shelf circulation. *Cont. Shelf Res.* **15**:155–128.

Bretherton, F.P., Davis, R.E. and Farber, M.S. (1975) A technique for the objective analysis and design of oceanographic experiments applied to MODE-73. *Deep-Sea Res.* **23**:559–582.

Colbourne, E.B., Helbig, J.A. and Cumming, D. (1993) Improved ADCP performance using a hydrodynamically designed boom mount. *J. Atmos. Oceanic Techn.* **10**:629–636.

Crombie, D.D. (1955) Doppler spectrum of sea echo at 13.56 MHz. *Nature* **175**:681–682.

Davidson, F. (1999) *Wind driven circulation in Trinity and Conception Bays*. PhD Thesis, Newfoundland: Memorial University of Newfoundland.

Denman, K.L. and Powell, T.M. (1984) Effects of physical processes on planktonic ecosystems in the coastal ocean. *Oceanogr. Mar. Biol. Annu. Rev.* **22**:125–168.

Ha, E.-C. (1979) *Remote Sensing of Ocean Surface Current and Current Shear by HF Backscatter Radar*. PhD Thesis, Stanford: Stanford University, 134p.

Hannah, C.G., Shore, J.A. and Loder, J.W. (2000) The drift-retention dichotomy on Browns Bank: a model study of interannual variability. *Can. J. Fish. Aquat. Sci.* **57**:2506–2518.

Heath, M. and Gallego, A. (1998) Bio-physical modelling of the early life stages of haddock, *Melanogrammus aeglefinus*, in the North Sea. *Fish. Oceanogr.* **7**:110–125.

Heath, M., Zenitani, H., Watanabe, Y., Kimura, R. and Ishida, M. (1998) Modelling the dispersal of larval Japanese sardine, *Sarinops melanostictus*, by the Kuroshio current in 1993 and 1994. *Fish. Oceanogr.* **7**:335–346.

Helbig, J.A. and Pepin, P. (1998a) Partitioning the influence of physical processes on the estimation of ichthyoplankton mortality rates I. Theory. *Can. J. Fish. Aquat. Sci.* **55**:2189–2205.

Helbig, J.A. and Pepin, P. (1998b) Partitioning the influence of physical processes on the estimation of ichthyoplankton mortality rates II. Application to simulated and field data. *Can. J. Fish. Aquat. Sci.* **55**:2206–2220.

Liese, J.A. (1984) The analysis and digital signal processing of NOAA's surface current mapping system. *IEEE J. Ocean. Eng.* **OE-9**:106–113.

Lynch, D.R., Gentlemen, W.C., McGillicuddy, D.J. and Davis, C.S. (1998) Biological/physical simulations of *Calanus finmarchicus* population dynamics in the Gulf of Maine. *Mar. Ecol. Prog. Ser.* **169**:189–210.

Mackas, D.L. and Denman, K.L. (1985) Plankton patchiness. Biology in the physical vernacular. *Bull. Mar. Sci.* **37**:652–674.

Markle, D.F. and Frost, L.A. (1985) Comparative morphology, seasonality, and a key to planktonic fish eggs from the Nova Scotian Shelf. *Can. J. Zool.* **63**:246–257.

McGillicuddy, D.J., Lynch, D.R., Moore, A.M., Gentleman, W.C., Davis, C.S. and Meise, C.J. (1998) An adjoint data assimilation approach to the diagnosis of physical and biological controls on Pseudocalanus spp. in the Gulf of Maine-Georges Bank region. *Fish. Oceanogr.* **7**:205–218.

Pepin, P., Dower, J.F., Helbig, J.A. and Leggett, W.C. (2002) Regional differences in mortality rates of a larval fish, the radiated shanny (*Ulvaria subbifurcata*): estimating the relative roles of dispersal and predation. *Can. J. Fish. Aquat. Sci.* **59**:105–114.

Pepin, P. and Helbig, J.A. (1997) Distribution and drift of Atlantic cod (*Gadus morhua*) eggs and larvae on the northeast Newfoundland shelf. *Can. J. Fish. Aquat. Sci.* **54**:670–685.

Pepin, P., Helbig, J.A., Laprise, R., Colbourne, E.B. and Shears, T.H. (1995) Variations in the contribution of transport to changes in planktonic larval abundance: a study of the flux of fish larvae in Conception Bay, Newfoundland. *Can. J. Fish. Aquat. Sci.* **52**:1475–1486.

Pepin, P. and Shears, T.H. (1997) Variability and capture efficiency of bongo and tucker trawl samplers in the collection of ichthyoplankton and other macrozooplankton. *Can. J. Fish. Aquat. Sci.* **54**:765–773.

Proctor, R., Wright, P.J. and Everitt, A. (1998) Modelling the transport of larval sandeels on the north-west European shelf. *Fish. Oceanogr.* **7**:347–354.

Roache, P.J. (1985) *Computational Fluid Dynamics*. Albuquerque, NM: Hermosa, 446pp.

Sinclair, M. (1988) *Marine Populations: An Essay on Population Regulation and Speciation*. Seattle, Washington: University of Washington Press.

Stewart, R.H. and Joy, J.W. (1974) HF radar measurements of surface currents. *Deep-Sea Res.* **21**:1039–1049.

Sundby, S. (1983) A one-dimensional model for the vertical distribution of pelagic fish eggs in the mixed layer. *Deep-Sea Res.* **30**:645–661.

Taggart, C.T. and Frank, K.T. (1990) Perspectives on larval fish ecology and recruitment processes: probing the scales of relationships. In: *Large Marine Ecosystems: Patterns, Processes, and Yields*. K. Sherman, L.M. Alexander and B.D. Bold (eds) Washington, DC: American Association for the Advancement of Science, pp. 151–164.

Taggart, C.T., Thompson, K.R., Maillet, G.L., Lochman S.E. and Griffin D.A. (1996) Abundance distribution of larval cod (*Gadus morhua*) and zooplankton in a gyre-like water mass on the Scotian Shelf. In: *Survival Strategies in Early Life Stages of Marine Resources*. Y. Watanabe, Y. Yamashita and Y. Oozeki (eds) Rotterdam: A.A. Balkema, pp. 155–173.

Werner, F.E., Perry, R.I., Lough, R.G. and Naimie, C.E. (1996) Trophodynamic and advective influences on Georges Bank larval cod and haddock. *Deep-Sea Res.* **43**:1793–1822.

deYoung, B., Greatbatch, R.J. and Forward, K.B. (1993a) A diagnostic coastal circulation model with application to Conception Bay, Newfoundland. *J. Phys. Oceangr.* **23**:2317–2365.

deYoung, B., Otterson, T. and Greatbatch, R.J. (1993b) The local and nonlocal response of Conception Bay to wind forcing. *J. Phys. Oceanogr.* **23**:2636–2649.

deYoung, B. and Sanderson, B.R. (1995) The circulation and hydrography of Conception Bay. *Atmos. Ocean* **33**:135–162.